Atmos. Chem. Phys., 11, 3211–3225, 2011
www.atmos-chem-phys.net/11/3211/2011/
doi:10.5194/acp-11-3211-2011

Atmospheric Chemistry and Physics

African biomass burning plumes over the Atlantic: aircraft based measurements and implications for H_2SO_4 and HNO_3 mediated smoke particle activation

V. Fiedler[1,2], F. Arnold[2,1], S. Ludmann[2], A. Minikin[1], T. Hamburger[1], L. Pirjola[3,4], A. Dörnbrack[1], and H. Schlager[1]

[1]Deutsches Zentrum für Luft- und Raumfahrt, Institut für Physik der Atmosphäre, Oberpfaffenhofen, 82234 Wessling, Germany
[2]Max-Planck Institute for Nuclear Physics, (MPIK), Atmospheric Physics Division, P.O. Box 103980, 69029 Heidelberg, Germany
[3]Department of Physics, University of Helsinki, P.O. Box 64, 00014 Helsinki, Finland
[4]Department of Technology, Metropolia University of Applied Sciences, P.O. Box 4000, 00180 Helsinki, Finland

Received: 18 February 2010 – Published in Atmos. Chem. Phys. Discuss.: 25 March 2010
Revised: 9 January 2011 – Accepted: 18 March 2011 – Published: 5 April 2011

Abstract. Airborne measurements of trace gases and aerosol particles have been made in two aged biomass burning (BB) plumes over the East Atlantic (Gulf of Guinea). The plumes originated from BB in the Southern-Hemisphere African savanna belt. On the day of our measurements (13 August 2006), the plumes had ages of about 10 days and were respectively located in the middle troposphere (MT) at 3900–5500 m altitude and in the upper troposphere (UT) at 10 800–11 200 m. Probably, the MT plume was lifted by dry convection and the UT plume was lifted by wet convection. In the more polluted MT-plume, numerous measured trace species had markedly elevated abundances, particularly SO_2 (up to 1400 pmol mol^{-1}), HNO_3 (5000–8000 pmol mol^{-1}) and smoke particles with diameters larger than 270 nm (up to 2000 cm^{-3}). Our MT-plume measurements indicate that SO_2 released by BB had not experienced significant loss by deposition and cloud processes but rather had experienced OH-induced conversion to gas-phase sulfuric acid. By contrast, a significant fraction of the released NO_y had experienced loss, most likely as HNO_3 by deposition. In the UT-plume, loss of NO_y and SO_2 was more pronounced compared to the MT-plume, probably due to cloud processes. Building on our measurements and accompanying model simulations, we have investigated trace gas transformations in the ageing and diluting plumes and their role in smoke particle processing and activation. Emphasis was placed upon the formation of sulfuric acid and ammonium nitrate, and their influence on the activation potential of smoke particles. Our model simulations reveal that, after 13 August, the lower plume traveled across the Atlantic and descended to 1300 m and hereafter ascended again. During the travel across the Atlantic, the soluble mass fraction of smoke particles and their mean diameter increased sufficiently to allow the processed smoke particles to act as water vapor condensation nuclei already at very low water vapor supersaturations of only about 0.04%. Thereby, aged smoke particles had developed a potential to act as water vapor condensation nuclei in the formation of maritime clouds.

Correspondence to: F. Arnold
(frank.arnold@mpi-hd.mpg.de)

1 Introduction

Biomass burning (BB) is a global phenomenon, which has an impact on the environment and climate (Crutzen et al., 1979; Andreae, 1983; Crutzen and Andreae, 1990; Houghton et al., 2001). BB plumes contain elevated concentrations of pollutants, including smoke particles and primary as well as secondary combustion gases. Savanna fires represent the single most important BB-type worldwide (Crutzen and Andreae, 1990; Andreae, 1991; Koppmann et al., 2005). Africa contains about two thirds of the world's savanna regions and 90% of the African savanna fires are believed to be human induced (Koppmann et al., 2005). Since BB plumes can be transported over thousands of kilometers, their impact on the environment and climate may occur far away from BB regions. For example, elevated O_3 present over the South

Atlantic has been attributed to secondary O_3 formation in BB plumes originating from Africa (see review by Koppmann et al., 2005; Real et al., 2010).

BB releases primary pyrogenic gases (Koppmann et al., 2005) and primary smoke particles (Table 1, see recent review by Reid et al., 2005), whose characteristics and relative emission rates depend on various factors including particularly the type of bio material combusted and the burning conditions (flaming, smoldering).

Primary pyrogenic gases include, besides the major combustion products H_2O and CO_2, numerous minor gases, particularly CO, hydrocarbons, NO, NH_3 and SO_2 (Andreae and Merlet, 2001). Interaction of NO and organics leads to the formation of secondary ozone, which represents a greenhouse gas, an important atmospheric oxidant, and a precursor of OH radicals.

Primary pyrogenic particles contain solid cores, mostly soot (elemental carbon (EC)) and ash, and a semi-volatile coating composed of low vapor pressure organics (organic carbon (OC)), which is formed by rapid OC-condensation. The resulting internally mixed smoke particles have initial median diameters of about 125 nm and a mass ratio OC/EC of about 5–10 (Reid et al., 2005).

As a BB burning plume ages and dilutes, chemical transformations of primary pyrogenic gases take place leading to secondary gases including particularly O_3. Some secondary gases undergo gas-to-particle conversion leading to chemical processing and additional size growth of primary smoke particles. Of these secondary gases, sulfuric acid (H_2SO_4) and nitric acid (HNO_3) are particularly important. Sulfuric acid is formed by OH-induced conversion of the primary pyrogenic gas SO_2 (Reiner and Arnold, 1993, 1994). Nitric acid is formed via OH-induced conversion of NO_2, which results from rapid conversion of primary pyrogenic NO. Due to its very low saturation vapor pressure, sulfuric acid condenses on smoke particles and, due to its very large hygroscopicity, tends to increase smoke particle hygroscopicity. Nitric acid has a much higher saturation vapor pressure than sulfuric acid and would condense on smoke particles only in conditions of temperatures below about 200 K, which are occasionally found only at the tropical tropopause and in the polar lower stratosphere. However, HNO_3 may react with gases possessing large proton affinities. A key candidate is the primary pyrogenic trace gas ammonia (NH_3), whose BB release is about ten times larger than that of SO_2 but only about half of that of NO_y. HNO_3 reacts with NH_3 yielding ammonium nitrate (NH_4NO_3), which is thermally stable at temperatures typical of the middle and upper troposphere. Therefore, after BB plume ascent to the middle troposphere NH_3 may undergo conversion to NH_4NO_3, which could then condense on smoke particles. Gas-phase sulfuric acid, which is more slowly formed than HNO_3, may convert some fraction of the NH_4NO_3, leading to aerosol-phase ammonium sulfate ($(NH_4)_2SO_4$). The HNO_3 not converted to NH_4NO_3, would remain in the gas-phase. Hence, the difference of NO_y and HNO_3 abundances sets an upper limit to the NH_4NO_3 abundance. It is also conceivable that primary and secondary organic acids may neutralize NH_3 yielding ammonium salts. In addition, NH_3 may also react with other pyrogenic gases, leading to amides and nitriles. Also, in the very early plume, NH_3 may undergo chemical conversion to NO_x increasing with BB fire temperature (Hegg et al., 1988).

However, smoke particles as well as the gases HNO_3, NH_3 and SO_2, the precursor of H_2SO_4, may experience substantial loss by cloud processes and deposition. Therefore, their concentrations in an aged BB plume and the effects on smoke particle processing by H_2SO_4 and HNO_3 are difficult to predict. Removal of SO_2 by cloud processes is only moderate since SO_2 dissolution in cloud droplets is only moderate. Importantly, ice clouds do not scavenge gas-phase SO_2. During droplet freezing dissolved SO_2 may even be released to the gas-phase (Clegg and Abbatt, 2001). However dissolved SO_2 may undergo H_2O_2 mediated liquid-phase conversion to sulfate, which remains in the aerosol-phase after cloud water evaporation.

By contrast to SO_2, the trace gases HNO_3 and NH_3 are highly soluble in cloud droplets and therefore may undergo very substantial removal by cloud processes. But, after convective ascent and cloud dissipation, additional HNO_3 can be photochemically formed from NO_x, which is not significantly removed by cloud processes. Efficient formation of NH_4NO_3 requires transport of NH_3 to the middle troposphere where temperatures are sufficiently low to allow thermal stability of NH_4NO_3 (see above). Therefore, efficient NH_4NO_3 formation in a middle troposphere air mass lifted by convection probably requires “dry convection”.

Considering typical emission factors (Table 1) a biomass burning event releases more NO_y than NH_3. If one neglects removal by deposition and cloud processes, in an air mass which has experienced dry convection to the middle troposphere, the following highly simplified picture evolves: Ultimately, more HNO_3 molecules may be formed than NH_3 molecules are present. Therefore, HNO_3 may neutralize NH_3, forming NH_4NO_3. Only the HNO_3 and NH_3 corresponding to the equilibrium partial vapor pressures of NH_4NO_3 will remain in the gas-phase. NH_4NO_3 will condense on the pyrogenic primary particles. The formation of gas-phase sulfuric acid from SO_2 is much slower than HNO_3 formation and the SO_2 released from biomass burning is about ten times less than the NH_3 released. Therefore, gas-phase sulfuric acid formed in the ageing middle troposphere plume will convert only some fraction of the particle-bound NH_4NO_3 to $(NH_4)_2SO_4$. Nevertheless, as mentioned above, the fraction of pyrogenic NH_3 reaching the middle and upper troposphere is highly uncertain.

Sulfuric acid, due to its large hygroscopicity, may have a particularly large effect on the ability of smoke particles to take up water molecules from the gas-phase in conditions with relative humidity $RH < 100\%$, and to act as water vapor condensation nuclei (CCN = cloud condensation nuclei)

Table 1. Emission factors Ex, molar emission ratios $E\mathrm{x}/E\mathrm{CO_2}$(adopted from Andreae and Merlet, 2001) and the measured excess molar emission ratio $d\mathrm{x}/d\mathrm{CO_2}$. The last column denoted with R gives the ratio between $d\mathrm{x}/d\mathrm{CO_2}$ and $E\mathrm{x}/E\mathrm{CO_2}$.

Substance x	Ex (g kg^{-1})	$E\mathrm{x}/E\mathrm{CO_2}$ (mol mol^{-1})	$d\mathrm{x}/d\mathrm{CO_2}$ (mol mol^{-1})	R
CO	65 ± 20	$6.3\times10^{-2} \pm 2.2\times10^{-2}$	4.3×10^{-2}	6.8×10^{-1}
TPM	8.3	5.1×10^{-3} g g^{-1}	$>2.5 \times10^{-3}$ g g^{-1}	$>4.9\times10^{-1}$
NO_y	3.9 ± 2.2	$3.5\times10^{-3} \pm 2.2\times10^{-3}$	6×10^{-4}	1.7×10^{-1}
NO_x	–	–	3.8×10^{-5}	–
PAN	–	–	9.2×10^{-5}	–
HNO_3	–	–	$3.8–6.9\times10^{-4}$	–
NH_3	0.6-1.5	$1.0\text{-}2.4\times10^{-3}$	$<1\times10^{-4}$	$<1\times10^{-1}$
SO_2	0.35 ± 16	$1.5\times10^{-4} \pm 0.7\times10^{-4}$	1×10^{-4}	6.7×10^{-1}
HCHO	0.26–0.44	$2.3–4.0\times10^{-4}$	7.7×10^{-5}	$3.3–1.9\times10^{-1}$
CO_2	1613	–	$d\mathrm{CO_2}=1.3\times10^{-5}$	–

in cloud formation in conditions with RH > 100%. Smoke particle processing by H_2SO_4 and NH_4NO_3 is particularly important for atmospheric conditions with only small water vapor supersaturations WSS of only about 0.05%, which are typical for the maritime boundary layer and for maritime stratiform cloud formation (Seinfeld and Pandis, 1998). The larger the H_2SO_4 mass fraction of a smoke particle, the smaller will be the activation water vapor supersaturation (WSSa) required for activation. The H_2SO_4 formed in the ageing plume increases with time until precursor SO_2 is exhausted. Therefore, also the H_2SO_4 mass fraction of smoke particles increases with time. As a consequence, the ability of a smoke particle of a given size to act as CCN (at a given water vapor supersaturation) increases with time as the H_2SO_4 mass fraction increases due to H_2SO_4 uptake (see also model simulations below). In addition, coagulation contributes to increase the smoke particle diameter, which also contributes to decrease the water vapor supersaturation required for activation. However, as the plume ages, the number concentration of smoke particles decreases strongly, due to coagulation and plume dilution. Therefore, the number concentration of smoke particles which can be activated, at a given WSS, is expected to have a maximum at a certain plume age. The larger the rate of SO_2-conversion to H_2SO_4, the smaller will be the plume age at which this maximum occurs and the larger will be the maximum concentration of smoke particles which can be activated.

Therefore, the rate of SO_2 conversion to gas-phase H_2SO_4 in the ageing and diluting plume is crucial in determining the H_2SO_4 mass fraction of smoke particles, and thereby the evolution of their activation potential. This rate is determined by the OH concentration and its time variation in the plume. In a BB plume, the OH concentration is thought to be controlled mostly by OH-loss via the reaction of OH with NO_2 leading to HNO_3 and by OH-formation via processes involving organic plume gases (preferably acetone-photolysis leading to about 3.2 HO_x radicals per acetone molecule) (Singh et al., 1994; Folkins et al., 1997). While elevated NO_x tends to decrease OH, increased acetone tends to increase OH. Previous measurements of OH in an aged BB plume at 9000–10 000 m altitude have indicated OH concentrations of about 0.1 pmol mol^{-1} (Folkins et al., 1997). These, were not much different from ambient OH concentrations outside the BB plume. This led to the conclusion that the additional NO_x-induced OH loss was approximately offset by an additional acetone-induced OH formation.

The present paper reports on airborne measurements of SO_2 and HNO_3 along with other gases and smoke particles in two aged savanna fire plumes over the East Atlantic, off the west coast of equatorial Africa (Gulf of Guinea). At the time of our measurements one plume was located in the middle troposphere (MT) and one in the upper troposphere (UT). From the trace gas data we infer the formation of H_2SO_4, HNO_3 and NH_4NO_3 in the plumes and discuss implications with regard to their influence on the smoke particle activation potential.

2 Experiment

Our airborne BB plume measurements were part of the AMMA (African Monsoon Multidisciplinary Analyses) campaign and took place on 13 August 2006, off the western coast of Tropical Africa (Ghana). The measurements were made by various instruments on board the DLR (Deutsches Zentrum für Luft- und Raumfahrt, German aerospace center, Oberpfaffenhofen) research aircraft Falcon, when it dived into and cruised in two plumes at altitudes between about 3900 and 5500 m and between 10 800 and 11 200 m.

The AMMA project aims at a better understanding of the West African Monsoon, its influence on the processing of chemical emissions and its associated regional-scale and vertical transports. For this purpose an airborne campaign was conducted in July/August 2006 with special interest on biomass burning emissions. Further objectives were the characterization of the impact of mesoscale convective systems on the ozone budget in the upper troposphere and the evolution of the chemical composition of these convective plumes as they move westward toward the Atlantic Ocean. Another objective was to discriminate the impact of remote sources of pollution over West Africa, including transport from the middle East, Europe, Asia and from southern hemispheric BB fires.

Sulfur dioxide (SO_2) was measured by a chemical ionization mass spectrometry (CIMS) method with continuous inflight calibration using isotopically labeled SO_2. The CIMS-instrument, which has been developed by MPI-K (Max-Planck-Institute for Nuclear Physics, Heidelberg) in collaboration with DLR, is equipped with a powerful ion trap mass spectrometer. A comprehensive description of the measurement system can be found in Speidel et al. (2007) and Fiedler et al. (2009a,b). The method is based on gas-phase ion molecule reactions in a flow reactor. These reactions involve reagent ions CO_3^- which react with atmospheric SO_2 ultimately leading to SO_5^- product ions. By measuring the abundance ratio of product and reagent ions with the ion trap mass spectrometer, the SO_2 mole fraction can be determined. The SO_2 measurements have a time resolution of 1 second and a detection limit (2 sigma level) of about 20 pmol mol^{-1}. The relative error is about plus or minus 12% for SO_2 mole fractions larger than 100 pmol mol^{-1} and increases close to the detection limit to plus or minus 40% (Speidel et al., 2007).

Nitric acid (HNO_3) measurements have been carried out with the same CIMS instrument. HNO_3 can be detected using the gas-phase ion molecule reaction of CO_3^- with HNO_3. This reaction leads to $(CO_3HNO_3)^-$ cluster ions, which again are detected by the mass spectrometer. The time resolution of the measurements is 1 s, the detection limit is 0.1 nmol mol^{-1} in our case, the estimated relative error plus or minus 50%, as we did not use a special HNO_3 calibration, but applied the SO_2 calibration instead. A detailed description of the further developed HNO_3 measurement method with HNO_3 calibration can be found in Jurkat et al. (2010).

Simultaneous measurements of other trace gases (CO_2, CO, NO, NO_y, H_2CO, O_3) were carried out on the Falcon by DLR (see Table 2).

Carbon monoxide (CO) was detected using vacuum resonance fluorescence in the fourth positive band of CO (Gerbig et al., 1999). The accuracy of the CO measurements is ±10% for a time resolution of 5 s and with a detection limit of 3 nmol mol^{-1}. Carbon dioxide (CO_2) was measured with a differential nondispersive infrared instrument (NDIR), the detection limit was 0.1 µmol mol^{-1}, the sampling rate 1 s and the accuracy ±0.1% (Schulte et al., 1997).

Nitric oxide (NO) and the sum of reactive nitrogen compounds (NO_y) were measured using a chemiluminescence technique (Schlager et al., 1997; Ziereis et al., 2000). The NO_y compounds are catalytically reduced to NO on the surface of a heated gold converter with addition of CO. The accuracy of the NO and NO_y measurements is ±8% and ±15%, respectively. The time resolution is 1 s and the detection limit 5 pmol mol^{-1} and 15 pmol mol^{-1}, respectively. The nitrogen-bearing trace gas NH_3 is not detected by the NO_y-instrument. Also ammonium nitrate is not measured, but the NO_y-instrument measures HNO_3 released from NH_4NO_3 by thermal decomposition, when atmospheric air is passed through the flow tube section containing the hot NO_y-converter of the NO_y-instrument.

Ozone (O_3) was measured using an UV absorption photometer (Schlager et al., 1997; Schulte et al., 1997). The accuracy of the ozone detection is ±5%, the detection limit is 1 nmol mol^{-1} and the time resolution 4 s. Formaldehyde H_2CO has been measured using a Hantzsch reaction instrument (Kormann et al., 2003). The detection limit of this instrument is 84 pmol mol^{-1}, the time resolution is 180 s and the uncertainty ±30% at a mixing ratio of 300 pmol mol^{-1}.

Table 2 compiles the measured atmospheric substances, measurement techniques, specifications of the techniques and corresponding references.

Number concentrations and size distribution of aerosol particles in the size range between 4 nm and 20 µm were measured with a combination of condensation particle counters and a differential mobility particle sizer mounted in the cabin, as well as two wing-mounted optical aerosol spectrometer probes in a similar setup described by Weinzierl et al. (2009). The instruments deployed on the DLR Falcon during AMMA are listed in more detail in the supplement of Reeves et al. (2010). The cabin instruments sampled air through the forward facing DLR Falcon aerosol inlet, which is operated close to isokinetic sampling conditions and has no significant sampling losses for particles up to 1.5 µm particle diameter. The size range of particles in the accumulation and coarse mode above approximately 0.15 µm particle size is covered by measurements of the PCASP-100X and the FSSP-300 wing probes, two instruments which in principle detect the amount of light scattered by single particles. In order to infer the particle size distribution, knowledge on the complex refractive index of the aerosol particles is required (Schumann et al., 2010). In this study, we used for simplicity an refractive index of 1.54 + 0.0i, commonly used to represent an aged ammonium sulfate type aerosol, for all size distribution data discussed. In particular for particles falling into the PCASP-100X size range (0.15–1.0 µm) the possible error introduced by this simplification is estimated to be below natural variability due to the instrument being relatively insensitive to variations in the actual refractive index. Particle concentrations in this manuscript are reported as ambient concentrations.

3 Plume localization and trajectories

Figure 1 depicts a MODIS (Moderate Resolution Imaging Spectroradiometer) image of fires in Africa for the period 1–10 August 2006. MODIS is an instrument on the

Table 2. Compilation of gas phase instruments deployed on the Falcon during AMMA. Also compiled are detection limits and uncertainties.

Substance	Method	Det. Limit (2σ) [$nmol\,mol^{-1}$]	Time resolution [s]	Accuracy [%]	Reference
SO_2	IT-CIMS	0.02	1	12	Speidel et al. (2007)
HNO_3	IT-CIMS	0.1	1	50	Jurkat et al. (2010)
NO	Chemiluminescence	0.005	1	8	Schlager et al. (1997)
NO_y	Chemiluminescence	0.015	1	15	Ziereis et al. (2000)
CO	Fluorescence	3	5	10	Gerbig et al. (1999)
CO_2	NDIR	100	1	0.1	Schulte et al. (1997)
H_2CO	Hantzsch reaction	0.084	180	30	Kormann et al. (2003)
O_3	UV absorption	1	4	5	Schlager et al. (1997)

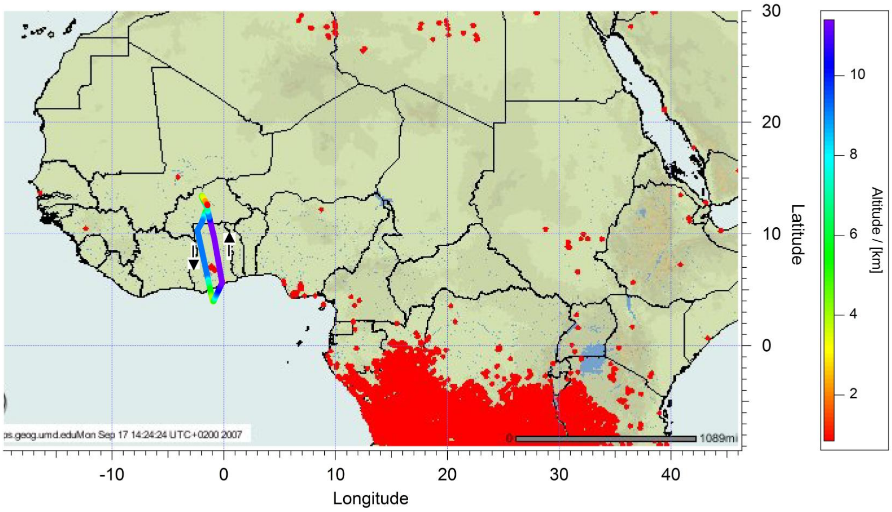

Fig. 1. Fires in Central Africa detected by MODIS (see text) for Northern Africa between the 1st and the 10th of August 2006. Also shown is the flightpath of the DLR research aircraft Falcon, color coded with flight altitude.

satellites TERRA and AQUA (Justice et al., 2002; Giglio et al., 2003; NASA/GSFC) and detects hotspots/fires as a thermal anomaly using data from the middle infrared and thermal infrared bands. In most cases, this thermal anomaly is a fire, but sometimes it is a volcanic eruption or the flare from a gas well. The minimum detectable fire size is a function of many different variables (scan angle, sun position, land surface temperature, cloud cover, amount of smoke and wind direction etc.), so the precise value slightly varies with these conditions. Results of validation measurements indicate that the minimum flaming fire size typically detectable at 50% probability with MODIS is on the order of 100 m^2. Under ideal conditions performance is somewhat better and the smallest detectable fire size is approximately 50 m^2. As can be seen from the figure, fires had been active in a large region covering the southern hemispheric African continent mostly south of the tropical rainforest belt, which suggests that most of the fires were savanna fires. The core of the BB region with the largest density of fire spots was located between about 20–30° East and 5–15° South. Also shown in Fig. 1 is the Falcon flight path with the flight altitude color coded. To probe the plume, the Falcon took off on 13 August 2006 at Ouagadougou (Burkina Faso, 12.35° N, −1.51° W) and flew at 9000–11 000 m altitude in southern direction to the equatorial Atlantic region off the coast of Ghana (western branch of the flight path in Fig. 1). Here it dived into the plume to a lowest height of 3900 m where it cruised for about 5 min. Hereafter it climbed out of the plume again and flew back to Ouagadougou (right branch of the flight path in Fig. 1). During that dive, the polluted air mass was even visible as a thick brownish layer. When looking downward, surface details were not visible.

Figure 2 shows an image of light absorbing aerosol particles measured on 13 August (day of our airborne measurements) by OMI (ozone monitoring instrument) aboard the AURA satellite (Levelt et al., 2006a,b). Plotted is the aerosol index AI, a product determined from the difference between the backscattered UV wavelength in a polluted atmosphere and a pure atmosphere (a positive AI values means absorbing aerosols). The OMI instrument can distinguish between

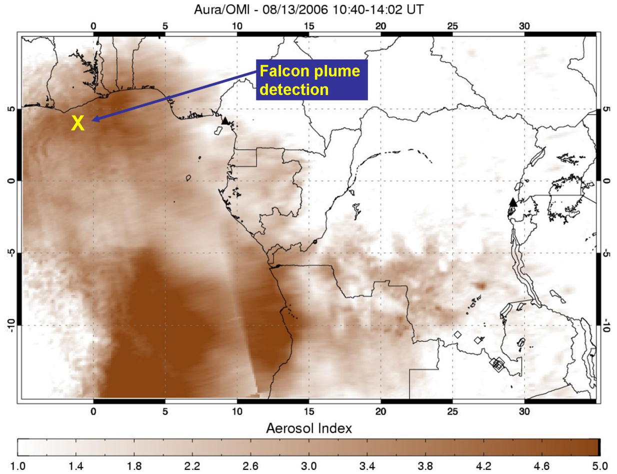

Fig. 2. Aerosol Index AI of light absorbing aerosols measured by OMI on Satellite AURA on the 13 August 2006.

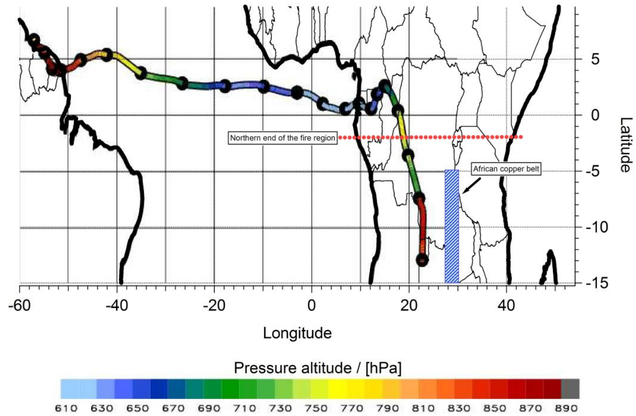

Fig. 3. Combination of the LAGRANTO 10-day back-trajectory starting at 13 August 2006 12:00 UTC with the LAGRANTO 10-day forward-trajectory starting at 13 August 2006 12:00 UTC. The color bar gives the air trajectory pressure. The red dots mark the northern edge of the fire region as shown in Fig. 1 and the blue area marks the so-called African copper belt.

aerosol types, such as smoke, dust and sulfates, and measures cloud pressure and coverage, which provide data to derive tropospheric ozone. The instrument employs hyperspectral imaging to observe solar backscatter radiation in the visible and ultraviolet. The instrument is a contribution of the Netherlands's Agency for Aerospace Programs (NIVR) in collaboration with the Finnish Meteorological Institute (FMI) to the Earth Observing System (EOS) Aura mission. The AI image (Fig. 2) reveals the presence of an extended pollution plume rich in light absorbing aerosol particles, mostly soot particles. The plume of light absorbing particles is present mainly over the Tropical East Atlantic and also over Tropical Africa and covers an area of at least 4 million km^2. Unfortunately, the height of the soot plume cannot be obtained from the satellite image. The plume exhibits a horizontally inhomogeneous distribution and the dive of the Falcon into the plume took place in one of the denser plume regions (dive region is marked by a cross in Fig. 2).

CALIPSO (**C**loud **A**erosol **L**idar and **I**nfrared **P**athfinder **S**atellite **O**bservations, see also http://www.nasa.gov/calipso) lidar data also confirm the presence of the middle troposphere plume (hereafter MT-plume) over the Gulf of Guinea, on 13 August. For the region of the Falcon dive into the MT-plume, they indicate a top altitude of about 5000 m and a bottom altitude of about 3000 m (Real et al., 2010).

To investigate the origin of the MT-plume, we have made back-trajectory simulations using the LAGRANTO model (Wernli and Davies, 1997). Figure 3 shows a typical 10-day back-trajectory of the lower plume superimposed on a map. The altitude of the trajectory is indicated by the color code. The time span between tick-marks (filled circles) is 24 h. Also shown on the map are the northern edge of the fire region as detected by MODIS between 1 and 10 August 2006 (red dots) and the African copper belt region (blue area). The so-called African copper belt is the region in Zaire and Zambia, where major copper smelters are located, which represent major SO_2 sources.

On 4 August, 10 days prior to our measurements, the air parcel, which was intercepted by the Falcon at 3900 m on 13 August, passed at about 1200 m altitude over the core of the fire region, about 500 km west of the copper-smelters. Hereafter, during 7–10 August, the air parcel traveled at about 4000 m altitude over the north western region of the fire belt. Hence, it seems that the air parcel took up pyrogenic gases mainly on 4 August when it passed at low altitudes over the core of the fire belt. This would imply a time span of 10 days for transit from the core of the BB region to the measurement region. On 5 August, while leaving the core of the BB region, the air parcel ascended from about 1200 m to about 3000 m and on 8 August it reached about 4000 m altitude.

We also investigated air mass trajectories starting from the copper-smelter region during the days of interest. We found out, that all air mass trajectories starting in the copper belt led to the North or even to the East. So an uptake of copper smelter SO_2 is not likely.

To investigate the fate of the MT-plume, after 13 August, we have also made LAGRANTO forward-trajectory model simulations. Therefore, Fig. 3 shows additionally to the 10-day back-trajectory a 10-day forward simulation of the trajectory, starting on 13 August at 3900 m altitude at 12:00 UTC. This simulation indicates that, after our measurements, the plume parcel traveled westward over the Atlantic and reached the coast of northern Brazil on 20 August. Hereafter it traveled northwards again. While reaching the Brazilian coast, the plume parcel descended to a lowest height of about 1300 m altitude.

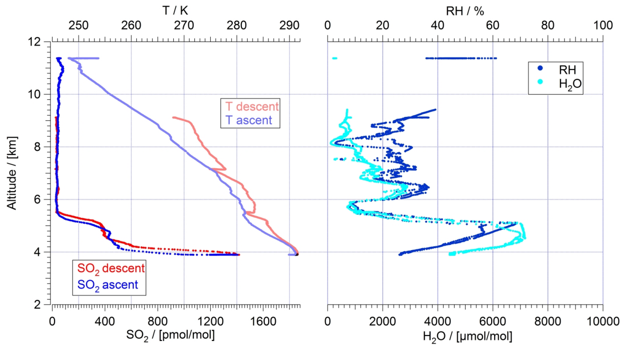

Fig. 4. Altitude profiles of the measured SO_2 mole fraction and the Temperature (first panel, measurements during the descent of the Falcon in red, during reascent in blue). Altitude profile of the measured water vapor concentration and relative humidity (second panel).

4 Measurement results

Figure 4 shows in its left panel the altitude profiles of SO_2 and temperature (both descents in red, ascents in blue). The altitude profile of the SO_2 mole fraction indicates the presence of a SO_2-rich plume in the mid troposphere (hereafter termed MT plume) with a sharp top at about 5200 m (descent) to 5000 m (ascent) and two altitude regimes with different degrees of SO_2 pollution, including an upper plume regime and a main plume regime (below about 4200 m). The Falcon has spent about 11 min inside the MT- plume, below 5200 m, corresponding to a horizontal distance of about 150 km. On that horizontal length scale the top altitude of the MT plume was quite similar, differing only by 200 m. As the Falcon ascended further, a pronounced local SO_2 maximum of about 90 pmol mol^{-1} was observed at 12:24 UTC. This indicates the presence of a second much less polluted plume in the UT at about 10 800–11 200 m altitude (hereafter termed UT-plume, Fig. 4). Its height extension was only about 400 m which is much less than that of the MT-plume (about 2000 m).

In the right panel of Fig. 4 water vapor concentration (H_2O) and relative humidity (RH) are shown. In the MT-plume, H_2O and RH are elevated. The absolute water vapor mole fraction reaches up to 7200 µmol mol^{-1}, in the upper part of the MT-plume in a layer between about 4400 and 5100 m. This indicates upward transport of humid air. Temperature reaches up to 292 K at about 4000 m and RH reaches up to 64%, in the upper part of the MT-plume, at 5000 m.

Figure 5, first and second panel, show the time series of measured trace gases (plotted are CO, CO_2 and O_3, NO_y, NO, HNO_3, and H_2CO). CO_2, which is widely used as biomass burning marker, is strongly enhanced inside the MT-plume. All trace gases are also markedly increased in the MT-plume. Within the MT-plume, at constant altitude of the Falcon of 3900 m, the trace gases HNO_3, NO and CO increase, whereas the other measured trace gases remain almost constant.

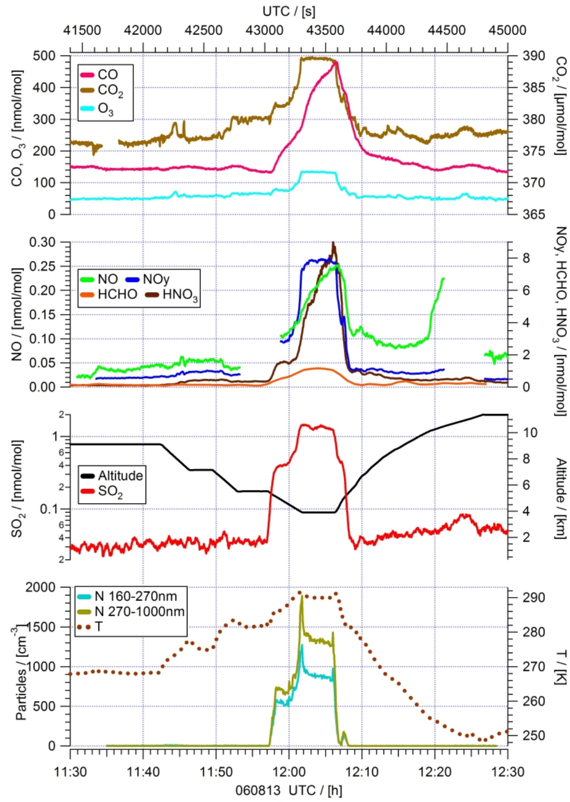

Fig. 5. Time sequences of measured atmospheric trace gases and particles. Panel 1: CO, CO_2 and O_3 mole fractions. Panel 2: NO, NO_y, H_2CO and HNO_3 mole fractions. Panel 3: SO_2 mole fraction and flight altitude. Panel 4: Number concentration of aerosol particles possessing diameters from 160 to 270 nm and from 270 to 1000 nm. Also given is the outside air temperature T. Between 11:57 and 12:08 UTC the pollution plume is detected in all trace gases and in the particles.

Figure 5, third panel, shows the time series of flight altitude and the SO_2 mole fraction measured by the CIMS-instrument. As the Falcon dived from 9000 to 5500 m, SO_2 increases slightly from about 30–40 pmol mol^{-1}. After a short cruise just above the top of the visible plume at 5500 m, the Falcon dived further to 3900 m. During that dive, between 5500 m to about 5000 m, SO_2 increases abruptly by a factor of about 10 to about 400 pmol mol^{-1}, and below about 5250 m, SO_2 further increases abruptly to 1400 pmol mol^{-1}. During the following short cruise at 3900 m, SO_2 varies between 1400 and 1250 pmol mol^{-1}. After that 5 min cruise at 3900 m, as the Falcon ascended, SO_2 decreases abruptly to 430 pmol mol^{-1}, and above 4700 m, SO_2 decreases further to the previous atmospheric background value of 30–40 pmol mol^{-1}, reached at 5700 m.

Aerosol particle time series data are shown in the forth panel of Fig. 5. Plotted are ambient number concentrations of aerosol particles possessing diameters between 160 and 270 nm ($N_{160-270}$) and between 270 and 1000 nm ($N_{270-1000}$). Also given is the outside air temperature during the measurements. As the Falcon dived in the MT-plume both aerosol particle concentrations increase very steeply and are correlated with SO_2 and the other trace gases. Pronounced maxima of particle concentrations were observed at 4–5 km altitude, just shortly before the Falcon had dived to the lowest altitude of 3900 m.

Figure 6 shows the corresponding altitude profiles of measured trace gases and particles. The shape of the altitude profile of NO_y is similar to SO_2, clearly showing an increase in the MT-plume. At 3900 m, NO_y reaches up to about 8 nmol mol^{-1} and the mole fraction ratio $d NO_y/d CO_2$ is about 6×10^{-4} (see Table 1). In the MT-plume at 3900 m, NO_x/NO_y is only 0.13 whereas the measured HNO_3/NO_y ranges between about 0.63 and 1.1. The trace gases CO, H_2CO and O_3 are markedly increased in the MT-plume. The trace gas H_2CO can be a primary pyrogenic gas and a secondary gas formed in the plume from primary gases. The gas O_3 represents a secondary gas formed in the plume via NO-oxidation by organics. For example, reaction of NO with the PA-radical (peroxyacetyl radical) leads to NO_2. Photolysis of NO liberates a single O-atom, which combines with O_2 to form O_3. The mole fraction ratio $d CO/d CO_2$, measured in the MT-plume at 3900 m is 0.043. The mole fraction ratio $d H_2CO/d CO_2$ measured in the MT-plume at 3900 m is 7.7×10^{-5}.

Aerosol particle number concentration altitude profiles are included in Fig. 6. Plotted are concentrations of particles possessing diameters of 4–1500 nm (N_4), 160–270 nm, 270–1000 nm, 500–1000 nm and 1000–5000 nm. In addition particles with diameters larger than 10 nm, which have been heated to 250 °C during passage of the thermo-denuder, are plotted and denoted N_{10} non-volatile. Hereafter, these particles will be termed "non-volatile (nv) particles". They most likely contain black carbon and ash and perhaps also certain organic carbon species with very low vapor pressures.

The N_4-altitude profile increases in the MT-plume with decreasing altitude, similar to SO_2. Above the MT-plume, N_4 increases with increasing altitude and reaches maximum values of about 1300 cm^{-3}. In the MT-plume, N_{10}(nv) is nearly identical to the total N_4. This indicates that in the plume almost all particles contain non-volatile cores. Above the MT-plume, most particles do not contain non-volatile cores.

The $N_{270-1000}$ are also very substantially increased in the MT-plume and during dive are as large as the N_4. This indicates that most particles had diameters larger than 270 nm. Of all measured trace substances, N_{270} exhibits the largest increase in the MT-plume at 3900 m (almost a factor of 1000).

The $N_{500-1000}$ profile also increases in the MT-plume (by a factor of about 100). The ratio $N_{500-1000}/N_{270-1000}$ is about 0.01 at 3900 m altitude.

$N_{1000-5000}$ is very small (0.1 cm^{-3}) at 3900 m. This indicates that clouds were absent, which is consistent with the relatively low RH (<27%) in the MT-plume at 3900 m altitude (see Fig. 4).

Summarizing the results of the altitude profiles, for SO_2, NO_y, H_2O, O_3, H_2CO and aerosol particles in the MT-plume, there were no notable differences between the ascent and descent data. In contrast, for CO, HNO_3 and NO, descent and ascent profiles are markedly different, ascent data (after the penetration of the plume) are larger. This increase of HNO_3, NO and CO during the cruise at the constant flight-level of about 3900 m altitude in the plume is puzzling. It contrasts the almost constant behavior of SO_2, NO_y, O_3 and CO_2. The increase of the abundance ratio of excess CO and excess CO_2 ($d CO/d CO_2$) could indicate a decrease of BB fuel carbon oxidation during combustion. Regarding HNO_3, pyrogenic ammonia (NH_3) may have reacted with HNO_3, yielding ammonium nitrate (NH_4NO_3), which condenses on primary particles. NH_4NO_3 formation may have occurred during adiabatic cooling of the ascending air mass and/or after ascent. Thermal decomposition of NH_4NO_3 in the sampling line of the CIMS instrument represents a potential source of gas-phase HNO_3. By contrast to HNO_3, NO_y (a major fraction of which is HNO_3) may not be affected by severe sampling line losses since in the NO_y instrument HNO_3 is rapidly converted to NO, which is much less sticky than HNO_3. Furthermore, the transfer line of the NO_y instrument is heated to a much higher temperature compared to the CIMS sampling line, which reduces wall losses.

Figure 7 shows two aerosol particle size distributions measured above the MT-plume in background conditions of the free troposphere at 4500 m (528 hPa) and in the MT-plume at 3900 m (645 hPa). The two size distributions are very different with the Aitken mode dominating in the background case and the accumulation mode inside the plume. Above the MT-plume the distribution is peaking at 40 nm. In the densest of the MT-plume at 3900 m, the size distribution is peaking at about 250 nm. This resembles the presence of fewer small particles and many more larger particles. The large particles are most likely aged smoke particles, which are substantially larger than typical primary smoke particles (median diameter: about 125 nm Reid et al., 2005). The relatively low particle concentrations below 100 nm particle diameter inside the plume indicate that entrained background aerosol particles must have experienced removal via coagulation with smoke particles, since coagulation with smoke particles becomes more efficient for smaller particles. It also implies that new particle formation is suppressed probably due to scavenging of gaseous sulfuric acid by aged primary smoke particles. The volume and mass concentrations of smoke particles can be inferred from the measured size distribution. Considering particles with diameters of up to 800 nm and assuming a specific weight of smoke particles of 1 g cm^{-3}, one obtains a smoke particle mass concentration of 6.5×10^{-11} g cm^{-3} (at 3900 m, 13 August, 12:04 UTC). These findings also compare very well to the results by de Reus et al. (2001).

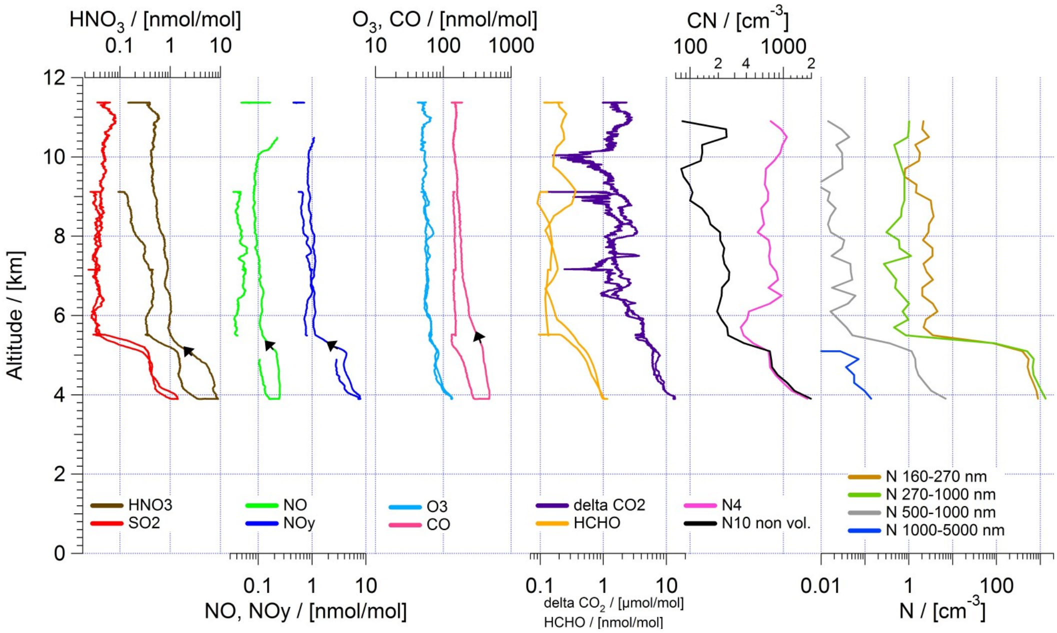

Fig. 6. Altitude profiles of SO_2, HNO_3, NO, NO_y, O_3, CO, CO_2, HCHO, and aerosol particle number concentrations N_x where the index x denotes the size range referred to in nm (N_{4-1500}, $N_{10-1500}$ (non-volatile particles), $N_{160-270}$, $N_{270-1000}$, $N_{500-1000}$ and $N_{1000-5000}$). For HNO_3, NO, and CO reascent data are markedly larger than descent data. For aerosol particles averaged profiles combining descend and ascend data using the median concentration of data in 100 m altitude bins are presented (no significant differences between descend and ascend observed).

5 Comparison with BB emission ratios

5.1 MT-plume

In the following, measured dX/dCO_2 and expected dx/dCO_2 (expected from savanna biomass burning) will be compared. The comparison will focus on the core of the MT-biomass burning plume penetrated by the Falcon at 3900 m around 12:06 UTC.

Molar ratios dX/dCO_2 of excess trace substance X and excess CO_2 (excess means measured value minus atmospheric background value), measured at 3900 m the MT-plume, are given in Table 1. Also given is the mass ratio $d\mathrm{TPM}/dCO_2$ (here TPM denotes total particle matter). Furthermore, for comparison, the corresponding published emission ratios for savanna fires are also given.

Concerning SO_2, the measured dSO_2/dCO_2 represents about 68% (average) of the molar emission ratio. The missing SO_2 must have been removed by reaction with OH and perhaps also by cloud processes. Considering only loss by OH-reaction (reaction rate coefficient of $1.5\times10^{-12}\,\mathrm{cm^3\,s^{-1}}$), one calculates tp $\times$ $\mathrm{OH_{eff}}$ $=$ $2.6\times10^{11}\,\mathrm{s\,cm^{-3}}$ (range: 0–$5.3\times10^{11}\,\mathrm{s\,cm^{-3}}$). Considering tp $=10$ days, one obtains $\mathrm{OH_{eff}}=3.0\times10^5\,\mathrm{cm^{-3}}$ (range: 0–$6.2\times10^5\,\mathrm{cm^{-3}}$). This mean $\mathrm{OH_{eff}}$ is somewhat smaller than the expected $5.0\times10^5\,\mathrm{cm^{-3}}$ (see above). This suggests that no substantial SO_2 removal occurred by processes other than OH reaction.

Concerning CO, the measured dCO/dCO_2 is almost equal to the molar emission ratio. The most important CO-loss is due to reaction with OH (rate coefficient: about $2\times10^{-13}\,\mathrm{cm^3\,s^{-1}}$ at $p=500$ hPa). Using the above $\mathrm{OH_{eff}}=3.0\times10^5\,\mathrm{cm^{-3}}$ inferred from SO_2, one obtains a mean CO-lifetime (against OH-reaction) of about 193 d. This implies that, after 10 days, about 95% of the initial CO should still be present, which is consistent with the observation, when uncertainties of the measured dCO and dCO_2 and the emission factors are considered.

The HNO_3 measured in the plume peak is almost equal to the measured NO_y. This implies that PAN and NH_4NO_3 were not very abundant. The measured dNO_y/dCO_2 represents about 46% of the molar emission ratio. The missing NO_y may have experienced loss by deposition. Probably, NO_y losses occurred mainly via HNO_3.

For the TPM concentration at 3900 m altitude, our inferred value of $6.5\times10^{-11}\,\mathrm{g\,cm^{-3}}$ (see above) implies a mass ratio $d\mathrm{TPM}/dCO_2=4.2\times10^{-3}\,\mathrm{g\,g^{-1}}$. The ratio of the emission factors for primary smoke particles and CO_2 is $5.1\times10^{-3}\,\mathrm{g\,g^{-1}}$. Hence it seems that the measured TPM concentration represents about 74% of the expected primary TPM concentration. Therefore, it seems that some loss of smoke particles by deposition and cloud processes may have occurred.

The observed H_2CO must be of secondary origin since, in clear sky conditions, H_2CO is rapidly lost by photolysis. This

(a)

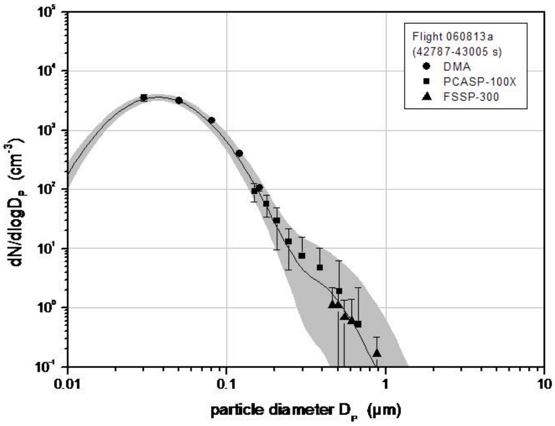

(b)

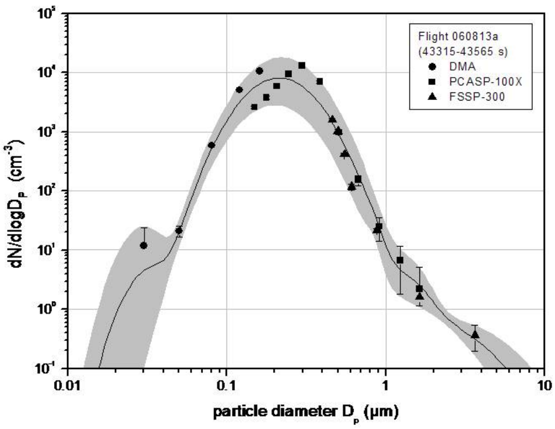

Fig. 7. Aerosol particle size distributions measured **(a)** above the MT-plume at 4500 m (528 hPa), and **(b)** in the MT-plume at 3900 m (645 hPa) altitude. Different symbols represent data points of different instruments (see legend). The line as well as the lower and upper end of the grey shaded area represent log-normal fits to the data (averaged, minimum, maximum concentrations within the integration time period).

seems to be consistent with dry convection. The 1/e-lifetime is only about 3 h, which is much smaller than the plume age. For example, H_2CO can be formed by O_2-reaction of the PA-radical.

5.2 UT-plume

The upper tropospheric plume (UT-plume) was probably uplifted by wet convection in the north-western Republic of Congo and the Central African Republic about 10 days prior to our measurements. This contrasts the transport of the MT-plume, which was uplifted south of the equator between 10 and 23 degrees south, where wet convection is much less probable and much less intense (see Real et al., 2010).

Regarding SO_2, 14–38% of the expected SO_2 have been observed (expected from the emission ratios), which is smaller compared to the MT-plume. This may indicate that a substantial fraction of the released SO_2 experienced loss by cloud processes.

The observed HNO_3 represents only about 3.4% of the expected NO_y. However, at the much lower temperature of the UT-plume, PAN is thermally stable and may contribute about half of the NO_y while HNO_3 may contribute the other half. If so, about 6.8% of the expected HNO_3 would have been present. Compared to the lower plume, this fraction of residing NO_y is still markedly smaller. This suggests more efficient HNO_3 removal by wet cloud processes. This is, at least qualitatively, consistent with the above mentioned wet convection induced uplift of the UT-plume.

Regarding aerosol particles, dN_4 is about 2 times dN_{10}(nv), which indicates that half of the enhanced particles contain non-volatile smoke particle cores and are not new particles formed in the UT by nucleation. This is at least qualitatively consistent with the relatively low total SO_2 (80 pmol mol^{-1}), which hardly allows sufficient H_2SO_4 formation required for H_2SO_4-H_2O nucleation (see for example Fiedler et al., 2009a).

6 Aerosol model simulations

To investigate the evolution between 4 and 24 August, of the smoke particle size, number concentration, H_2SO_4-mass fraction, and the critical (minimum) water vapor super saturation required for smoke particle activation (WSSa), we have made model simulations (AEROFOR model, Pirjola, 1999; Pirjola and Kulmala, 2001; Pirjola et al., 2003). The model assumes smoke particles with an initial uniform diameter of 125 nm and an initial number concentration of 2.2×10^5 cm^{-3}. This number concentration was calculated considering an expected $d\mathrm{TPM}/d\mathrm{CO}_2 = 5.1 \times 10^{-3}$ g g^{-1}, a $d\mathrm{TPM} = 6.5 \times 10^{-11}$ g cm^{-3} measured on 13 August in the MT-plume at 3900 m, and an initial dTPM calculated from the measured dTPM , a specific weight of 1 g cm^{-3}, and taking an 1/e-time of 6.4 days for plume dilution. This dilution time was taken from Real et al. (2010). The plume parcel trajectory and meteorological data were taken from the LAGRANTO model. The trajectory is composed of two segments, a back-trajectory segment (4–13 August) and a forward-trajectory segment (13–24 August).

The model treats the following processes: mutual smoke particle coagulation (coagulation with entrained background particles is neglected); OH-induced SO_2-conversion to H_2SO_4; uptake of H_2SO_4 (plus associated H_2O) by smoke particles. The model is tuned to reproduce the SO_2 concentration (1.4 nmol mol^{-1}) measured on 13 August at 3900 m. Uptake of H_2SO_4 and sulfate entrained into the plume from the background atmosphere is neglected. For the period 4–13 August, the $OH_{eff} = 6.2 \times 10^5$ cm^{-3}, inferred from the observation on 13 August (at 3900 m), of 45% of the expected maximum SO_2 (see above) was considered. The

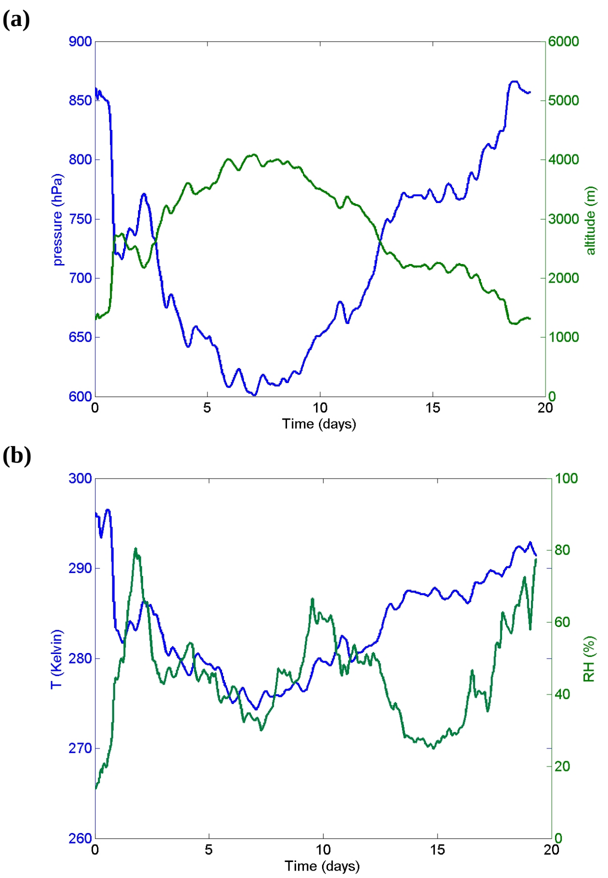

Fig. 8. (a) Time sequences of the atmospheric pressure and pressure altitude of the air parcel intercepted by the Falcon on 13 August at 3900 m for the entire simulation period of 20 days (4-24 August). **(b)** Time sequences of temperature and relative humidity.

corresponding noon-time OH is about $2.0\times10^{6}\,cm^{-3}$. For the period tp = 0–24 d (13–24 August), OH was taken from Logan et al. (1981). The model does not consider NH_4NO_3.

Figure 8a shows, for the entire simulation period of 20 days (4–24 August), time sequences of the atmospheric pressure and pressure altitude of the air parcel intercepted by the Falcon on 13 August at 3900 m.

Figure 8b shows for the same case as Fig. 8a the outside air temperature T and RH. T varies between about 275 and 297 K. T measured aboard the Falcon (290 K) markedly exceeds the modeled value (280 K). This discrepancy may be due to additional heating via light absorption by soot containing smoke particles. RH varies between about 8 and 50%. The largest local maxima of about 50% are reached during the initial ascend at tp = 2 d and during the final ascend at tp = 20 d. Water vapor supersaturation (RH > 100%), according to the model, was never reached.

Figure 9 shows time sequences of the modeled molecular number concentrations of OH, SO_2, and gas-phase H_2SO_4. Also given is a curve representing an inert plume dilution tracer having the same initial concentration as SO_2. Both, OH and gas-phase H_2SO_4 exhibit a pronounced diurnal variation. The SO_2 concentration curve exhibits a weak diurnal variation and decreases with time much more steeply than the plume dilution tracer. This indicates that SO_2-depletion was preferably due to OH-induced SO_2-conversion to gas-phase H_2SO_4.

Figure 10 shows a time sequence of number concentrations of smoke particles (N_{sp}) in the plume parcel (left axis of Fig. 10). N_{sp} decreases with increasing plume age tp, due to coagulation and plume dilution. Initially coagulation dominates and later, as N_{sp} has decreased sufficiently, coagulation becomes slow and plume dilution dominates. For tp = 10 days (13 August), the model N_{sp} is $1000\,cm^{-3}$, which is smaller than measured N_{sp} ($2000\,cm^{-3}$). After 20 days, N_{sp} has decreased to about $200\,cm^{-3}$.

Figure 10 additionally shows a time sequence of the smoke particle wet diameter D_{sp} for two cases: without and with binary H_2SO_4-H_2O condensation (right axis of Fig. 10). Without binary H_2SO_4-H_2O condensation, D_{sp} increases to 450 nm (tp = 10 d) and 470 nm (20 d), due to mutual smoke particle coagulation. With binary H_2SO_4-H_2O condensation, as tp increases, D_{sp} increases to 490 nm (tp = 10 d) and 545 nm (20 d), due to mutual smoke particle coagulation plus binary H_2SO_4-condensation. For tp = 10 d (13 August), the modeled D_{sp} = 450 nm (without binary H_2SO_4-H_2O condensation) is close to the peak dry D_{sp} (about 400 nm) of the experimental aerosol volume size distribution.

Figure 11 shows a time sequence of the mass concentrations of the primary smoke particle components (EC + OC), and the secondary components H_2SO_4, and H_2O (left axis of Fig. 11). The EC + OC curve decreases by a factor of about 20, due to plume dilution. On day 1, the H_2SO_4 curve increases steeply and on days 3–6 reaches a maximum of about $6000\,ng\,m^{-3}$. Hereafter until tp = 13 d the H_2SO_4 curve decreases only moderately, and ultimately it decreases more steeply. The H_2O mass fraction of smoke particles varies, mostly in response to the variability of RH.

Figure 11 additionally shows a time sequence of the H_2SO_4-mass fraction of smoke particles (right axis of Fig. 11). It exhibits a slight diurnal variation but generally increases throughout the simulation period. At tp = 10 d (13 August) it is about 9% and at tp = 24 d (24 August) it is about 14%.

7 Smoke particle activation

Modeled WSSa as function of modeled diameters and H_2SO_4-mass fractions of smoke particles, for six time steps tp (1, 2, 4, 6, 10, 24 days) are given in Fig. 12. Here it is assumed that H_2SO_4 would have the same effect on WSSa as NH_4NO_3 (for which the figure was originally plotted, see Seinfeld and Pandis, 1998). Hence, if the only soluble material contained in the smoke particles was H_2SO_4, WSSa would

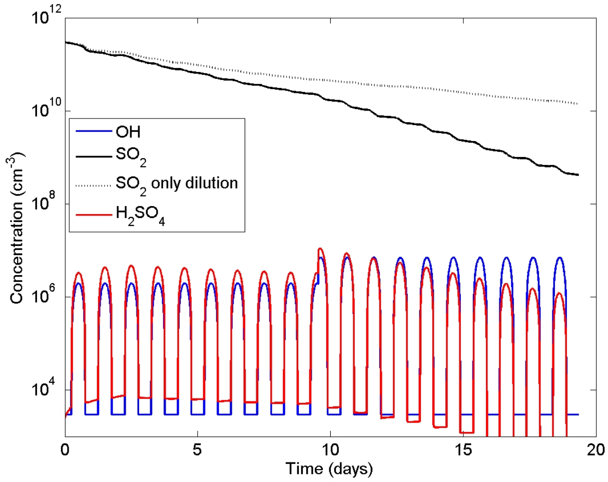

Fig. 9. Time sequences of the modeled molecular number concentrations of OH, SO_2 and gas-phase H_2SO_4. Also given is a curve representing an inert plume dilution tracer having the same initial concentration as SO_2 (SO_2 only dilution).

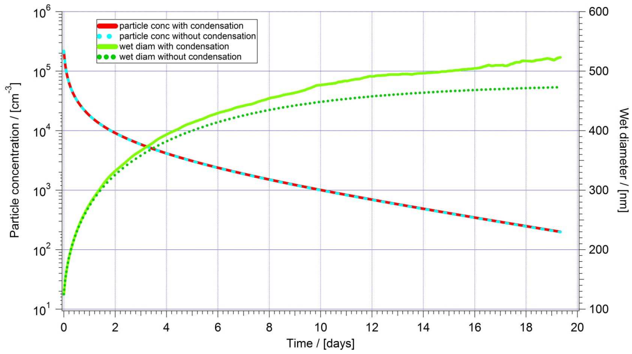

Fig. 10. Time sequence of the modeled number concentrations of smoke particles in the plume parcel, with and without considering condensation (left axis). Time sequence of the modeled smoke particle diameter D_{sp} for two cases: without and with binary $H_2SO_4-H_2O$ condensation (right axis).

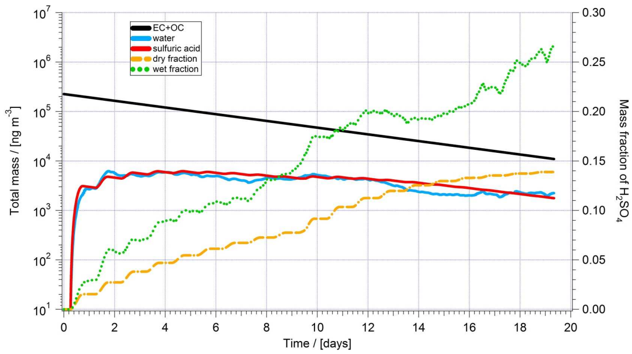

Fig. 11. Time sequence of the modeled mass concentrations of the primary smoke particle components (EC+OC), and the secondary components H_2SO_4 and H_2O (left axis). Time sequence of the modeled H_2SO_4 wet and dry mass fraction of smoke particles (right axis).

decrease with tp from about 0.3% (tp = 1 d) to about 0.033% (tp = 24 d), red crosses. Also included are values for the sum mass fraction of H_2SO_4 and NH_4NO_3 as blue crosses. In this case WSSa decreases to about 0.025% (tp = 24 d).

In comparison, WSS involved in maritime cloud formation are about 0.3–0.8% (cumulus clouds) and about 0.05% (maritime stratiform clouds). Hence, H_2SO_4-processed smoke particles contained in the plume parcel under consideration have developed a potential for maritime cumulus cloud formation (after 1 day) and for maritime stratiform cloud formation (after 10 days).

However, the modeled RH (Fig. 8b never exceeded 100% in the plume parcel under consideration. It is conceivable that small fluctuations, which are not considered by the model, may have resulted in small WSS, particularly at tp when the modeled RH was large.

The critical (minimum) WSS required for smoke particle activation (WSSa) decreases with increasing smoke particle diameter and increasing mass fraction of soluble material contained in the smoke particle (see Fig. 12). Conceivable smoke particle components, which are particularly efficient in this regard, are the secondary species H_2SO_4 and NH_4NO_3. The hygroscopicity of the semi-volatile organic coating of primary smoke particles is not well known. This organic coating may contain water soluble species as for example salts of organic acids. Organic acids may have experienced conversion to salts by reaction with primary pyrogenic NH_3. However, it is also conceivable that much of the organic coating is hydrophobic.

Sulfuric acid is formed in the plume via OH-induced conversion of SO_2 (see above). The 1/e-lifetime of SO_2 is determined by the OH-concentration which can be quite variable and is difficult to predict, particularly for the MT-plume where attenuation of solar UV-radiation and complex organic chemistry complicate modeling of OH. If particles and SO_2 would not be removed at different rates, the ratio of the sulfur mass concentration and primary particle mass concentration would remain equal to the ratio of the corresponding mass emission factors (mean value: 0.175/8.3 = 0.021) g S/g PSP; PSP denotes primary smoke particles). If the released SO_2 would ultimately be completely converted to H_2SO_4, the ratio of the H_2SO_4-mass concentration and primary smoke particle mass concentration would be about 0.065 g H_2SO_4/g PSP. Considering the ranges of expected emission factors for SO_2 and TPM, one obtains an ultimate ratio ranging from 0.025 to 0.153 g H_2SO_4/g PSP.

Nitric acid is formed in the plume by OH-induced conversion of NO_2. The NO_2-lifetime against OH-reaction is about 4 days when the above inferred OH_{eff} of 3.0×10^5 $cm^{-3}$is considered. However, NO_x is present not only as NO_2 but

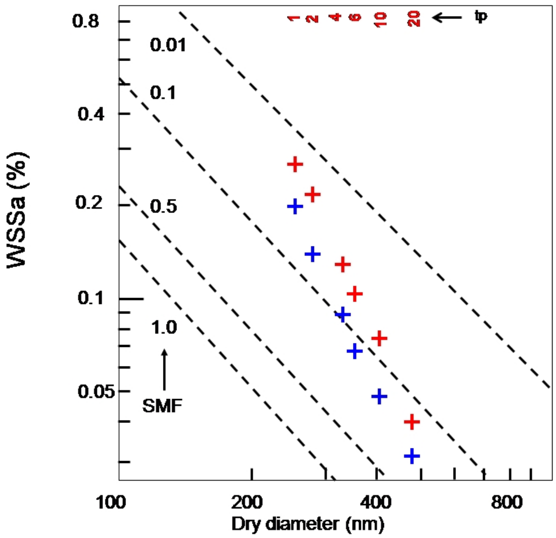

Fig. 12. Critical water vapor supersaturation WSSa as function of aerosol particle dry diameter (nm) for different NH_4NO_3 soluble mass fractions (SMF = 0.01, 0.1, 0.5, 1.0) (adopted from Seinfeld and Pandis, 1998). The crosses denote modeled WSSa as function of modeled diameters and H_2SO_4-mass fractions of smoke particles, for six time steps tp (1, 2, 4, 6, 10, 24 days) for the plume parcel intercepted on 13 August 2006 at 3900 m altitude. H_2SO_4 only: red cross; H_2SO_4+NH_4NO_3: blue cross.

also as NO. Therefore the NO_x-lifetime against conversion to HNO_3 is larger, depending on the abundance ratio NO_2/NO_x. For example, for an assumed $NO_2/NO_x = 0.5$, one obtains an NO_x-lifetime of about 8 days, which is much smaller than the SO_2-lifetime. This would imply that after 10 days $d\mathrm{NO_x}/d\mathrm{CO_2}$ decreased to only about 29% of its initial value.

Hence, HNO_3 was formed first and may have converted NH_3 and ammonium salts to NH_4NO_3. However, NH_4NO_3 may become thermally stable only after sufficient cooling of the plume, after it had ascended to about 3900 m, on 8 August. For example, in the plume at 3900 m, ($T = 290$ K, and relative humidity RH = 25%), NH_4NO_3 should be solid and the NH_4NO_3 dissociation equilibrium constant is about 4.9 nmol mol^{-1} × nmol mol^{-1} (for an atmospheric pressure of 630 hPa at 3900 m). This implies that the equilibrium mole fractions for each HNO_3 and NH_3 are about 2.4 nmol mol^{-1}. In comparison, the measured HNO_3 mole fraction is about 8 nmol mol^{-1}. The upper limit NH_3 mole fraction expected from the NH_3 emission ratio (see Table 1) is about 4 nmol mol^{-1}, if removal of (NH_3 + NH_4) would have been the same as NO_y-removal. This implies that the expected NH_3 exceeds the equilibrium NH_3 by about 2 nmol mol^{-1}. Therefore, about 2 nmol mol^{-1} of solid NH_4NO_3 may have been present, containing about 25% of the total NO_y. This is not in conflict with our observations when uncertainties of experimental data and BB emission factors are considered.

Considering the above estimated NH_4NO_3 mole fraction, the mass fractions of dry smoke particle components would become 7.07% (H_2SO_4), 8.3% (NH_4NO_3), and 15.4% (H_2SO_4 + NH_4NO_3). If this soluble material (NH_4NO_3 plus H_2SO_4) would have the same decreasing effect on WSSa as NH_4NO_3, WSSa would be lowered to about 0.05%, for a smoke particle with a diameter of 480 nm initially not containing soluble material (see Fig. 12).

However, as suggested by the trajectory model, after 13 August, the plume descended again and T and RH increased somewhat, which tends to lower the NH_4NO_3 associated with smoke particles. On the other hand, ongoing SO_2-conversion to GSA (Fig. 9) tends to increase the H_2SO_4-H_2O mass associated with smoke particles.

Hence, it seems that in the MT-plume, smoke particle processing by H_2SO_4 and NH_4NO_3 may have had a marked effect on the smoke particle activation potential. It also seems that, in the aged MT-plume on 19 August, H_2SO_4 was more important than NH_4NO_3 in increasing the activation potential of smoke particles.

8 Summary and conclusions

The main findings of the reported airborne BB plume measurements are:

a. An about 10 days old BB plume, located at about 3900–5500 m altitude, has been probed above the eastern Atlantic (Gulf of Guinea).

b. The plume originated from BB fires in the Southern-Hemisphere African savanna belt.

c. The plume was lifted by dry convection and had greatly elevated abundances of gas-phase and particle-phase pollutants.

d. The gases SO_2 (precursor of H_2SO_4) and HNO_3, which have a potential to mediate smoke particle activation had measured mole fractions of up to 1400 and 9000 pmol mol^{-1}.

e. Our data indicate that a large part of NO_y experienced loss probably via HNO_3 by deposition.

f. SO_2 did not experience a marked loss.

g. As the plume was ageing and diluting, SO_2 experienced OH-induced conversion to H_2SO_4, which induced rapid binary (H_2SO_4-H_2O)-condensation on smoke particles.

h. H_2SO_4 condensation, besides coagulation size growth, increased the activation potential of smoke particles. Also NH_4NO_3 formation may have contributed somewhat to increase the activation potential.

i. After 13 August (day of our measurements), the plume traveled over the Atlantic while descending to 1300 m altitude after 8 days. On 19 August it reached the west coast of south America (French Guyana) and hereafter traveled northward over the Atlantic.

j. On 19 August, smoke particles had a potential to become activated already at a very small WSS of only 0.05%, which would allow them to act as CCN in maritime stratiform cloud formation.

k. Another much less polluted BB plume observed at 10.8–11.2 km altitude was lifted by wet convection. It had experienced more efficient removal of SO_2, NO_y and particles probably by wet cloud processes.

Acknowledgements. Based on a French initiative, AMMA was built by an international scientific group and is currently funded by a large number of agencies, especially from France, UK, US and Africa. It has been the beneficiary of a major financial contribution from the European Community's Sixth Framework Research Programme. Detailed information on scientific coordination and funding is available on the AMMA International web site http://www.amma-international.org. We are furthermore grateful to the crew of the DLR Flight Department for their commitment and support to collect this data set. We also thank our colleagues Michael Lichtenstern, Paul Stock, Anke Roiger (DLR) and Bernhard Preissler, Ralph Zilly (MPI-K) for their support in instrument operation. This work was funded by DLR, MPI-K and Metropolia University of Applied Sciences, Helsinki.

The service charges for this open access publication
have been covered by the Max Planck Society.

Edited by: P. Formenti

References

Andreae, M.: Soot carbon and excess fine potassium: Long-range transport of combustion-derived aerosols, Science, 220, 1148–1151, 1983.

Andreae, M.: Biomass burning: Its history, use, and distribution and its impact on environmental quality and global climate, in: Global biomass burning: Atmospheric, climatic, and biospheric implications, MIT press, Cambridge, MA, London, 3–21, 1991.

Andreae, M. and Merlet, P.: Emission of trace gases and aerosols from biomass burning, Global Biogeochem. Cy., 15, 955–966, 2001.

Clegg, S. and Abbatt, J.: Uptake of Gas-Phase SO_2 and H_2O_2 by Ice Surfaces: Dependence on Partial Pressure, Temperature, and Surface Acidity, J. Phys. Chem. A, 105, 6630–6636, 2001.

Crutzen, P. and Andreae, M.: Biomass burning in the tropics: Impact on atmospheric chemistry and biogeochemical cycles, Science, 250, 1669–1678, 1990.

Crutzen, P., Heidt, L., Krasnec, J., Pollock, W., and Seiler, W.: Biomass burning as a source of atmospheric gases CO, H_2, N_2O, CH_3Cl and COS, Nature, 282, 253–256, 1979.

de Reus, M., Krejci, R., Williams, J., Fischer, H., Scheele, R., and Ström, J.: Vertical and horizontal distributions of the aerosol number concentration and size distribution over the northern Indian Ocean, J. Geophys. Res., 106, 28629–28641, doi:10.1029/2001JD900017, 2001.

Fiedler, V., Arnold, F., Schlager, H., Dörnbrack, A., Pirjola, L., and Stohl, A.: East Asian SO_2 pollution plume over Europe - Part 2: Evolution and potential impact, Atmos. Chem. Phys., 9, 4729–4745, doi:10.5194/acp-9-4729-2009, 2009a.

Fiedler, V., Nau, R., Ludmann, S., Arnold, F., Schlager, H., and Stohl, A.: East Asian SO_2 pollution plume over Europe - Part 1: Airborne trace gas measurements and source identification by particle dispersion model simulations, Atmos. Chem. Phys., 9, 4717–4728, doi:10.5194/acp-9-4717-2009, 2009b.

Folkins, I., Wennberg, P., Hanisco, T., Anderson, J., and Salawitch, R.: OH, HO_2, and NO in two biomass burning plumes: Sources of HO_x and implications for ozone production, Geophys. Res. Lett., 24, 3185–3188, 1997.

Gerbig, C., Schmitgen, S., Kley, D., Volz-Thomas, A., Dewey, K., and Haaks, D.: An improved fast-response vacuum-UV resonance fluorescence CO instrument, J. Geophys. Res., 104, 1699–1704, 1999.

Giglio, L., Descloitres, J., Justice, C. O., and Kaufman, Y. J.: An Enhanced Contextual Fire Detection Algorithm for MODIS, Remote Sens. Environ., 87, 273–282, 2003.

Hegg, D., Radke, L., and Hobbs, P.: Ammonia emissions from biomass burning, Geophys. Res. Lett., 15, 335–337, 1988.

Houghton, J. T., Ding, Y., Griggs, D. J., Noguer, M., van der Linden, P. J., Dai, X., Maskell, K., and Johnson, C. A.: Intergovernmental Panel on Climate Change (IPCC): Climate Change 2001, Cambridge Univ. press, 2001.

Jurkat, T., C., V., Arnold, F., Schlager, H., Aufmhoff, H., Schmale, J., Schneider, J., Lichtenstern, M., and Dörnbrack, A.: Airborne stratospheric ITCIMS measurements of SO_2, HCl, and HNO_3 in the aged plume of volcano Kasatochi, J. Geophys. Res., 115, D00L17, doi:10.1029/2010JD013890, 2010.

Justice, C., Giglio, L., Korontzi, S., Owens, J., Morisette, J., Roy, D., Descloitres, J., Alleaume, S., Petitcolin, F., and Kaufman, Y.: The MODIS fire products, Remote Sens. Environ., 83, 244–262, 2002.

Koppmann, R., von Czapiewski, K., and Reid, J. S.: A review of biomass burning emissions, part I: gaseous emissions of carbon monoxide, methane, volatile organic compounds, and nitrogen containing compounds, Atmos. Chem. Phys. Discuss., 5, 10455–10516, doi:10.5194/acpd-5-10455-2005, 2005.

Kormann, R., Fischer, H., de Reus, M., Lawrence, M., Brühl, Ch., von Kuhlmann, R., Holzinger, R., Williams, J., Lelieveld, J., Warneke, C., de Gouw, J., Heland, J., Ziereis, H., and Schlager, H.: Formaldehyde over the eastern Mediterranean during MINOS: Comparison of airborne in-situ measurements with 3D-model results, Atmos. Chem. Phys., 3, 851–861, doi:10.5194/acp-3-851-2003, 2003.

Levelt, P., Hilsenrath, E., Leppelmeier, G., van den Oord, G., Bhartia, P., Tamminen, J., de Haan, J., and Veefkind, J.: Science Objectives of the Ozone Monitoring Instrument, IEEE T. Geosci. Remote, 44, 1199–1208, 2006a.

Levelt, P., van den Oord, G., Dobber, M., Mälkki, A., Visser, H., de Vries, J., Stammes, P., Lundell, J., and Saari, H.: The Ozone Monitoring Instrument, IEEE T. Geosci. Remote, 44, 1093–1101, 2006b.

Logan, J., Prather, M., Wofsy, S., and McElroy, M.: Tropospheric

Chemistry: A Global Perspective, J. Geophys. Res., 86, 7210–7254, 1981.

NASA/GSFC: MODIS Hotspot / Active Fire Detections Data set. MODIS Rapid Response Project, http://maps.geog.umd.edu, last access: April 2011.

Pirjola, L.: Effects of the increased UV radiation and biogenic VOC emissions on ultrafine aerosol formation, J. Aerosol Sci., 30, 355–367, 1999.

Pirjola, L. and Kulmala, M.: Development of particle size and composition distribution with a novel aerosol dynamics model, Tellus, 53B, 491–509, 2001.

Pirjola, L., Tsyro, S., Tarrason, L., and Kulmala, M.: A monodisperse aerosol dynamics module – a promising candidate for use in the Eulerian long-range transport model, J. Geophys. Res., 108, 4258, doi:10.1029/2002JD002867, 2003.

Real, E., Orlandi, E., Law, K. S., Fierli, F., Josset, D., Cairo, F., Schlager, H., Borrmann, S., Kunkel, D., Volk, C. M., McQuaid, J. B., Stewart, D. J., Lee, J., Lewis, A. C., Hopkins, J. R., Ravegnani, F., Ulanovski, A., and Liousse, C.: Cross-hemispheric transport of central African biomass burning pollutants: implications for downwind ozone production, Atmos. Chem. Phys., 10, 3027–3046, doi:10.5194/acp-10-3027-2010, 2010.

Reeves, C. E., Formenti, P., Afif, C., Ancellet, G., Attié, J.-L., Bechara, J., Borbon, A., Cairo, F., Coe, H., Crumeyrolle, S., Fierli, F., Flamant, C., Gomes, L., Hamburger, T., Jambert, C., Law, K. S., Mari, C., Jones, R. L., Matsuki, A., Mead, M. I., Methven, J., Mills, G. P., Minikin, A., Murphy, J. G., Nielsen, J. K., Oram, D. E., Parker, D. J., Richter, A., Schlager, H., Schwarzenboeck, A., and Thouret, V.: Chemical and aerosol characterisation of the troposphere over West Africa during the monsoon period as part of AMMA, Atmos. Chem. Phys., 10, 7575–7601, doi:10.5194/acp-10-7575-2010, 2010.

Reid, J. S., Eck, T. F., Christopher, S. A., Koppmann, R., Dubovik, O., Eleuterio, D. P., Holben, B. N., Reid, E. A., and Zhang, J.: A review of biomass burning emissions part III: intensive optical properties of biomass burning particles, Atmos. Chem. Phys., 5, 827–849, doi:10.5194/acp-5-827-2005, 2005.

Reiner, T. and Arnold, F.: Laboratory flow reactor measurements of the reaction $SO_3 + H_2O + M \rightarrow H_2SO_4 + M$: Implications for gaseous H_2SO_4 and aerosol formation in the plume of jet aircraft, Geophys. Res. Lett., 20, 2659–2662, 1993.

Reiner, T. and Arnold, F.: Laboratory investigations of gaseous sulfuric acid formation via $SO_3 + H_2O + M \rightarrow H_2SO_4 + M$: Measurements of the rate constant and products identification, J. Chem. Phys., 101, 7399–7407, 1994.

Schlager, H., Konopka, P., Schulte, P., Schumann, U., Ziereis, H., Arnold, F., Klemm, M., Hagen, D. E., Whitefield, P. D., and Ovarlez, J.: In situ observations of air traffic emission signatures in the North Atlantic flight corridor, J. Geophys. Res., 102, 10739–10750, 1997.

Schulte, P., Schlager, H., Ziereis, H., Schumann, U., Baughcum, S., and Deidewig, F.: NOx emission indices of subsonic long-range jet aircraft at cruise altitude: In situ measurements and predictions, J. Geophys. Res., 102, 21431–21442, 1997.

Schumann, U., Weinzierl, B., Reitebuch, O., Schlager, H., Minikin, A., Forster, C., Baumann, R., Sailer, T., Graf, K., Mannstein, H., Voigt, C., Rahm, S., Simmet, R., Scheibe, M., Lichtenstern, M., Stock, P., Rüba, H., Schäuble, D., Tafferner, A., Rautenhaus, M., Gerz, T., Ziereis, H., Krautstrunk, M., Mallaun, C., Gayet, J.-F., Lieke, K., Kandler, K., Ebert, M., Weinbruch, S., Stohl, A., Gasteiger, J., Groß, S., Freudenthaler, V., Wiegner, M., Ansmann, A., Tesche, M., Olafsson, H., and Sturm, K.: Airborne observations of the Eyjafjalla volcano ash cloud over Europe during air space closure in April and May 2010, Atmos. Chem. Phys., 11, 2245–2279, doi:10.5194/acp-11-2245-2011, 2011.

Seinfeld, J. and Pandis, S.: Atmospheric Chemistry and Physics, John Wiley & Sons, Inc., first edn., 1998.

Singh, H., O'Hara, D., Herlth, D., Sachse, G., Blake, D., Bradshaw, J., Kanakidou, M., and Crutzen, P.: Acetone in the atmosphere: Distribution, sources, and sinks, J. Geophys. Res., 99, 1805–1819, 1994.

Speidel, M., Nau, R., Arnold, F., Schlager, H., and Stohl, A.: Sulfur dioxide measurements in the lower, middle and upper troposphere: Deployment of an aircraft-based chemical ionization mass spectrometer with permanent in-flight calibration, Atmos. Environ., 41, 2427–2437, 2007.

Weinzierl, B., Petzold, A., Esselborn, M., Wirth, M., Rasp, K., Kandler, K., Schutz, L., Koepke, P., and Fiebig, M.: Airborne measurements of dust layer properties, particle size distribution and mixing state of saharan dust during samum 2006, Tellus B, 61, 96–117, doi:10.1111/j.1600-0889.2008.00392.x, 2009.

Wernli, H. and Davies, H.: A Lagrangian-based analysis of extratropical cyclones. I: The method and some applications, Q. J. Roy. Meteorol. Soc., 123, 467–489, 1997.

Ziereis, H., Schlager, H., Schulte, P., van Velthoven, P., and Slemr, F.: Distributions of NO, NOx, and NOy in the upper troposphere and lower stratosphere between 28° and 61° N during POLINAT 2, J. Geophys. Res., 105, 3653–3664, 2000.